Third International Symposium on the Effects of Surface Geology on Seismic Motion
Grenoble, France, 30 August - 1 September 2006
Paper Number: xxx

VARIATIONS OF PEAK GROUND MOTIONS DUE TO SLIP HISTORIES: APPLICATION TO THE NEWPORT INGLEWOOD FAULT, LOS ANGELES BASIN

Haijiang Wang[1], Heiner Igel[1], Alain Cochard[1], Michael Ewald[1]
1 Department of Earth and Environmental Sciences, Ludwig-Maximilians-University of Munich, Germany

ABSTRACT - Finite-fault source inversions reveal the spatial complexity of earthquake slip over the fault plane. In this study, several possible earthquake scenarios of Mw 7.0 are simulated with different quasi-dynamic finite source models for the Newport Inglewood (NI) fault system in the Los Angeles (LA) basin embedded in the 3-D SCEC community velocity model version 3. We make use of the recently developed Numerical Green's Functions method (Wang *et al*., 2006) and synthesize ground motions from a data base of 3-D Green's functions, calculated for a discretized model of the NI fault. This allows efficient simulation of arbitrary slip histories. We investigate the effects of the various slip histories on peak ground velocities and the related uncertainties in ground motion prediction for our study area. The results confirm that the fault perpendicular components of motion are dominated by directivity effects while the fault parallel component is influenced both by the slip distribution and the basin structure.

1. Introduction

A major goal of hazard related seismology is to be capable of providing strong ground motions that can be used in engineering analyzes (Aki and Richard, 2002). However, this goal is hard to achieve because there are not sufficient observations of ground motions in zones at risk of large earthquakes to satisfy the demands of modern earthquake engineering practice, especially for the region close to major active faults. With the development of modern computer technology, the numerical method for calculation of the full wave-field will complement these demands and play a more and more central role in reliably estimating shaking hazard (e.g., Olsen and Archuleta, 1996; Olsen, 2000, Ewald *et al*., 2006). The main influences on ground motions can be split into two phenomena: (1) 3-D wave propagation effects from the fault to the station through the crust; (2) intrinsic source effects resulting from the diversity of fault slip histories. While the first effect can be continuously improved by incorporating new results from tomographic tools and/or direct measurements (e.g., borehole information), the uncertainty concerning source behavior remains and it is unquestionable that hazard relevant ground motion characteristics for earthquakes of a given size will strongly depend on rupture properties such as directivity, static slip, rupture speed, and rise time.

Thus it appears useful to estimate ground motions due to many "characteristic earthquakes" of a specific seismically active region with different slip scenarios, in order to account for rupture related ground motion variations. To achieve this goal we developed the concept of Numerical Green's Functions (NGF) (Wang et al., 2006): Green's functions

for discrete models of one fault or fault system for areas with sufficiently well known velocity structure are generated and stored in a database allowing arbitrary finite source scenarios to be synthesized at very little computational costs compared to complete 3-D calculations (this comes at the cost of the initial calculations of the 3-D NGFs).

The directivity effect has recently been given more attention by seismic engineers in the near-source region seismic motion prediction since it has a first order effect on ground motion (Anderson, 2003). It was first suggested to explain the accelerograms of the 1966 Parkfield earthquake (Aki, 1967; Haskell, 1969). Kinematic finite source simulations in a homogeneous medium were carried out to investigate source related effects (e.g. Archuleta and Hartzell, 1981; Anderson and Luco, 1983 a,b). In the region towards which the rupture propagates, the fault perpendicular component was found to have the strongest absolute amplitude. Somerville *et al.* (1997) develop empirical ground motion prediction relations based on several strong motion observations.

At the same time, some source parameters (static slip, rupture velocity, rise time, slip velocity) are found not to be uniform on the fault plane. Images of the spatial and temporal evolution of earthquake slip on fault planes provide compelling evidence that fault displacement is spatially variable at all resolvable scales, as also inferred from inversions of geodetic data (Larsen *et al*., 1992; Bennett *et al*., 1995). Investigations of strong ground motion also indicate the spatial variability of the rupture velocity (Archuleta, 1984; Beroza and Spudich, 1988; Bouchon *et al*., 2000). Herrero and Bernard (1994) proposed a model in which the rise time depends on the wave number of a spatially variable slip distribution. This source physics complexity appeals for thorough description of the source process when calculating seismic motion.

Those two contributions to ground motion variations are investigated in this paper. The concept of the NGF method is briefly introduced at first. It is then applied to the Newport Inglewood fault, located inside the best investigated area of the world— the Los Angeles basin area. The resulting database is used to synthesize different slip histories in order to provide a possible ground motion range for one hypothetical earthquake of Mw7.0. Using the pseudo-dynamic approach of Guatteri *et al*. (2005) for generating realistic rupture scenarios, 20 different slip histories are created and ground motions at the surface of the study area are synthesized. We characterize the resulting seismic shaking with maximum and mean values, as well as standard deviation of all the 20 resulting peak ground velocity (PGV) distributions. This allows a quantitative discussion of 3-D structural vs. source related effects.

2. The Theory of Numerical Green's Function method

The fundamental idea of the Numerical Green's Function method comes from the numerical solution of the representation theorem (e.g., Aki and Richard, 2002) which also forms the mathematical basis of another broadly used ground motion synthesization method - Empirical Green's Functions (e.g., Joyner and Boore, 1986; Hutchings and Wu, 1990; Bour and Cara, 1997; Kohrs-Sansorny *et al*., 2005). The target fault (immersed in a 3D velocity structure) is uniformly divided into rectangular sub-faults for which the Green's functions are separately calculated with a double-couple point source (restricted here to pure strike-slip) and stored afterwards. The slip-rate time function takes the form of a delta function which, after appropriately time-shifted and individually weighted, can sum up to generate the whole slip history of one sub-fault during the earthquake. The calculations can be carried out using any numerical solution to the 3-D wave propagation problem. Here we employ a high-order staggered-grid finite-difference approach (e.g., Igel *et al*.,

1995; Gottschämmer *et al.,* 2001) with efficient absorbing boundaries based on the concept of perfectly matched layers (e.g., Collino and Tsogka, 2001; Marcinkovich *et al*., 2003).

We thus provide the basic relation used to sum the Numerical Green's Functions in order to calculate the j-th component of velocity motion, $v_j(\mathbf{x},t)$, on the surface at an arbitrary position $\mathbf{x}$ at time *t* (which is similar to the numerical solution of the representation theorem given in Bour and Cara, 1997):

$$v_j(\mathbf{x},t) = \sum_{i=1}^{N} g_{ij}(\mathbf{x}, t+\tau_i-\tau_i^0) * s_i(\tau_i) \cdot \mu_i \cdot A_i \,, \qquad (1)$$

The j-th component of the Green's function excited by the i-th sub-fault is denoted as g_{ij}. The linear combination of those Green's functions is carried out over all N active sub-faults. The temporal variable τ_i is relative to the origin time and τ_i^0 represents the traveling time of the rupture front from the hypocenter to the centre of the i-th sub-fault. The convolution over time incorporates the fact that the rupture at each point takes a finite amount of time to reach its final value. Every g_{ij}, calculated with a double-couple strike-slip source with a unit scalar moment of 1 N·m, is convolved by the slip-rate function of the i-th sub-fault, $s_i(\tau_i)$, which is scaled with the local shear modulus μ_i and the sub-fault surface A_i. The overall sum of the sub-fault moments adds up to the total moment M_{tot} of the finite-source earthquake, $M_{tot} = \sum_{i=1}^{N} \mu_i D_i A_i$, D_i being the total slip of the i-th sub-fault.

3. Study area—Newport Inglewood fault in the Los Angeles basin

Considering the media effect on wave propagation, an area of choice for our study is the Los Angeles (LA) basin for which several studies have been carried out and produced a reliable velocity structure. The Newport Inglewood fault system (NI), shown in Figure 1, is chosen as target fault to apply the NGF method because: (1) it hosted the M6.4 Long Beach earthquake in 1933 (Hauksson and Gross, 1991), causing serious damage; (2) it is still considered the most probable source for a damaging earthquake to the LA area; (3) the near-vertical plane can be approximated by a vertical plane to first order in the numerical calculations and the predominant right-lateral slip can be approximated with a pure strike-slip mechanism (Grant *et al.*, 2004). The fault has a length around 79 km. Thus a rectangular area of 110×100×30 km, in the two horizontal and vertical directions, is selected as study area, and rotated with such an angle that the longer side is parallel to the fault (see Figure 1). The velocity model is derived as the elastic part of the SCEC 3-D velocity model for the Los Angeles basin (Version 3, Kohler *et al*., 2003). To reduce the computational effort and the size of the finally created data base we limit the seismic velocities to values above 1.4 km/s. With a grid-length of 300 m implemented within the 3-D staggered finite-difference method, ground motion with frequency less than 0.5 Hz is usable which means the artificial numerical dispersion could be neglected. This will of course limit the applicability of this method. Nevertheless the main purpose of this study is to present a specific application of a methodology (NGFs) that in the future will allow a quantitative estimate of source-dependent ground motion variations in realistic 3-D media.

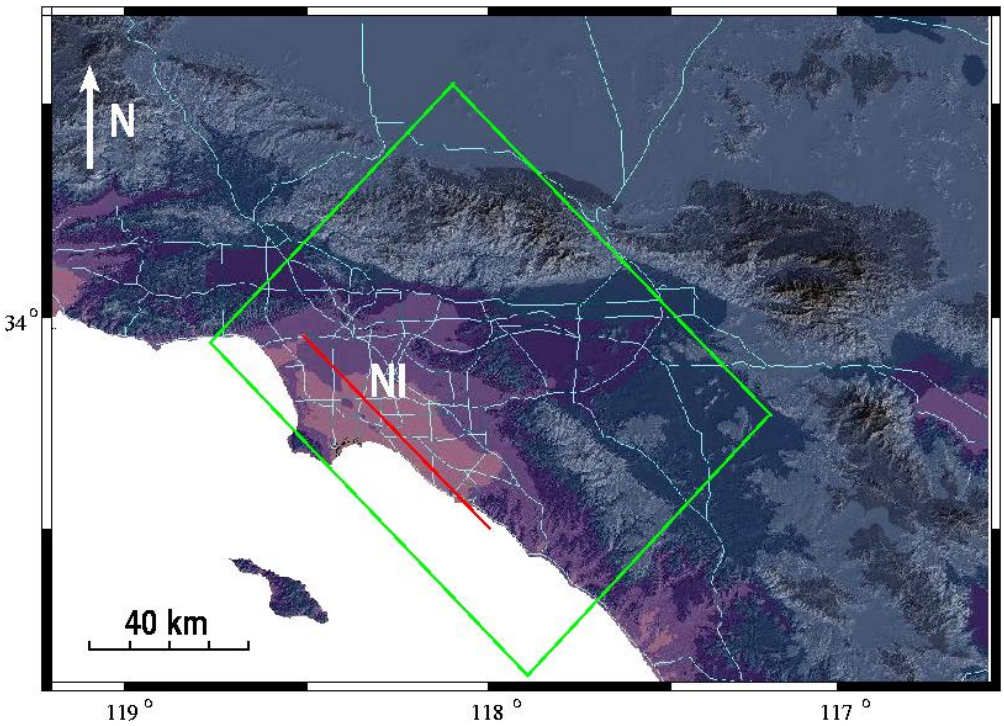

Figure 1. Los Angeles area with model region (green rectangular) and Newport Inglewood fault trace (NI, red line) where the color scale shows elevation above sea level.

When calculating the Green's functions, all grid points occupied by one sub-fault are sliding at the same time with the same pattern. The resulting discontinuous behavior - compared to the continuous solution - will introduce errors into the ground motion synthesization. These errors were investigated in detail in Wang *et al*. (2006) concluding that the accuracy of the synthesized ground motions gets better with increasing magnitude and rupture speed, and decreasing cut-off frequency of calculated seismograms. Based on these trends, they determine an optimal sub-fault size of 1.5 km (side-length) for Mw 7.0 earthquakes on the NI fault embedded in 3-D velocity structure of Los Angeles basin (shear wave velocity truncated at 1.4 km/s) and for frequencies no larger than 0.5 Hz.

4. Ground motion variations in 3-D due to slip histories

Huge variation of strong ground motion observed in the near-source can be described and explained with several phenomena like directivity, near-source impulse, and static offsets, which are strongly affected by the geometrical and dynamic characteristics of the faulting. In order to understand those phenomena and the associated uncertainties, how the ground motion varies with many different slip histories is worthy of an investigation. In the following sections we first describe the set up of the synthetic experiment, describe the source processes and analyze the resulting ground motions.

4.1. Slip histories

In this study, we synthesize 20 different "characteristic earthquakes" with magnitude Mw 7.0 with the forward NGF method to investigate source related variations. The fault length L and area *A* are calculated using the relationship by Wells and Coppersmith (1994), log L

= -2.57 + 0.62 M_w and log A = -3.42 + 0.9 M_w, and the scalar moment M_0 is related to magnitude through the empirical relation introduced by Kanamori (1977). The final average slip D is linked to the scalar moment, M_0, shear modulus μ , and fault area A by $M_0 = \mu DA$. Since no surface faulting was observed in the 1933 Mw 6.4 Long beach earthquake, the Mw 7.0 earthquake is also assumed to be buried inside the crust and the top edge of the fault is set at 1.8 km in depth.

The method published in Guatteri *et al.* (2005) is adopted to generate the quasi-dynamic rupture processes including the accelerating trends of the crack front due to the dynamic loading from the rupture area. The phenomenon that local high stress drop promotes fast rupture propagation is also accounted for. In this method, the final slip distribution is generated randomly with a given isotropic autocorrelation length (5 km). Rupture velocity and rise times are calculated as a function of the fault displacement and the hypocenter. The hypocenter remains fixed in order to focus on the ground motion variations due to slip histories. The shear velocity relevant for the slip histories is kept constant at 3.2 km/s and the rupture velocity is restricted to the range [0.6, 0.8] times shear velocity. The 20 final slip distributions calculated with this method are shown in Figure 2.

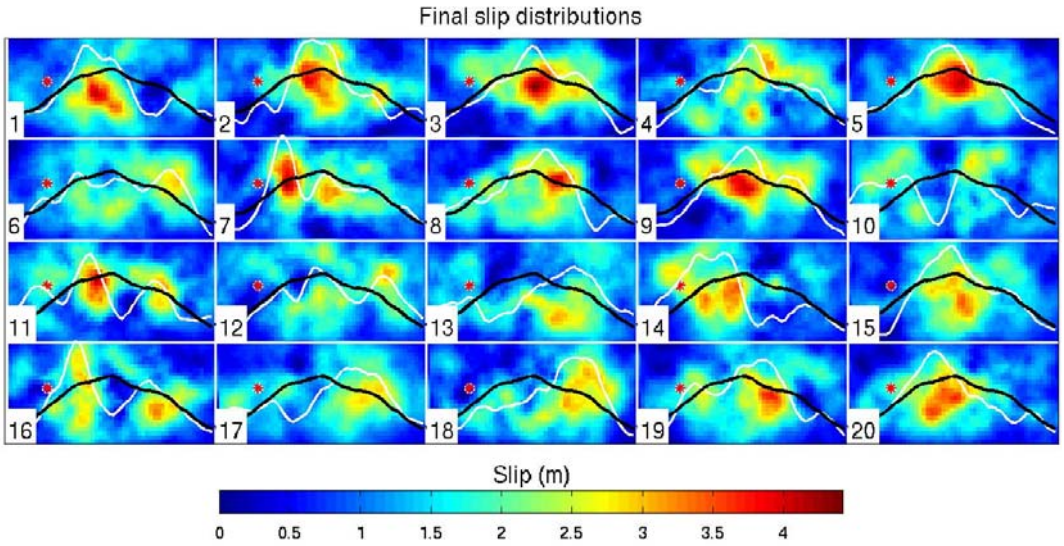

Figure 2: Numbered slip histories used in the simulations. Red stars mark the hypocenters. White and black lines show the comparison of single cumulative slip to the mean cumulative slip (of all slip histories), respectively. Slip histories are derived following Guatteri et al. (2005). Fault dimensions are 39×18 km, in strike and dip direction.

4.2. Average PGV characteristics for earthquake scenarios

First, the effect on different components of ground motion is illustrated in Figure 3 with mean values of all 20 PGV distributions on the surface for three components. The area, with mean PGV of y-component larger than 0.8 m/s (black rectangular, Figure 3, middle), is the area towards which the rupture propagates and where directivity plays the most obvious role. We name that area A. The maximum value of mean PGV in this area A for the y-component (fault perpendicular) is around 1.7 m/s, and almost twice larger than that for the x-component (fault parallel) and almost three times larger than that for the vertical component (note the different color scale). At the same time elevated mean PGV is observed inside the basin but outside area A both in the x-component and the vertical

component indicating the influence of basin structure and the slip variation. Thus it can be concluded that the fault perpendicular component is dominated by the directivity effect and the fault parallel and vertical components have significant contribution from the 3-D structure (basin effects) and slip distribution.

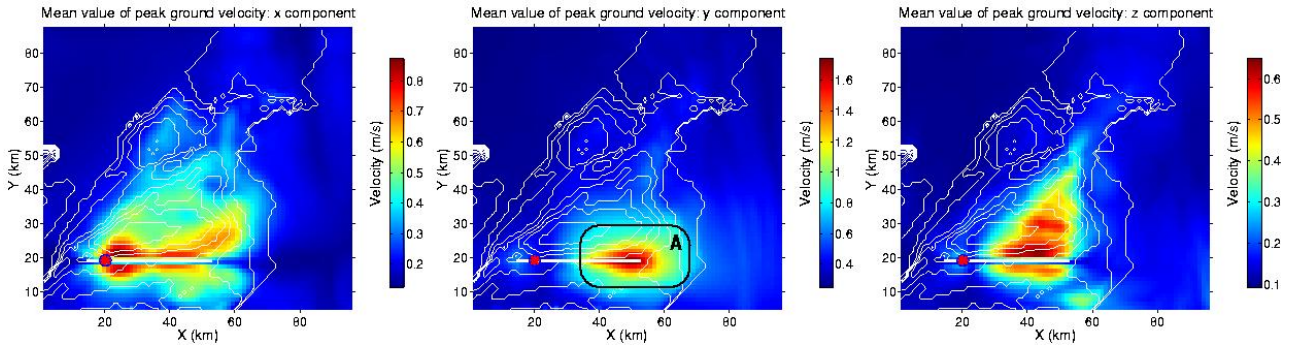

Figure 3: Mean value of PGV distributions from 20 different slip histories. From left to right are the fault parallel, fault perpendicular, and vertical velocity components. The thick white line is the fault trace on which red stars mark the epicenters. The thin white lines are the contours of the shear-wave velocity isosurface at 2 km/s Area A, black rectangular, shows the region where different directivity effect on different velocity component is observed

4.3. Source dependent PGV variations

To study the effects of various slip histories in more detail we take four different slip histories as example and show the resulting PGV distributions (Figure 4). These four slip histories are considered to be representative and their slip distributions are shown in the top of Figure 4. Slip 5 has a distinct asperity area right in the middle of the fault. Slip 7 has a smaller asperity area with very large slip close to the hypocenter. Slip 10 has a more uniformly distributed slip. Slip 16 has two asperity areas and the major part is located in the bottom half part of the fault. For slip 16, seismic motions have smaller amplitudes compared to the other three slip models because the most part of slip occurs in the bottom half part and further from the surface. Slip 5 gives a large PGV in the region close to its high slip asperity, especially in the x-component, indicating that large seismic motion is expected in the area close to asperities. This effect can also be seen in the results of slip 10 — there is a low PGV band between two high PGV areas along the fault plane that coincide with low cumulative slip as indicated in Figure 2. This may also be responsible for the sharp increase in PGV (y-component) beyond the area of low cumulative slip. Comparison of different components of PGV between the area inside the basin but far from the fault, and the area, A, close to the fault, suggests that the directivity plays a more important role on the component perpendicular to the fault plane.

Considering the complex PGV distribution on the surface due to different slip histories, it is instructive to present the possible range, namely maximum and variation (standard deviation), of shaking deduced from the 20 earthquakes for the NI fault. We show those ground motion characteristics in Figure 5. To give a further illustration of the directivity effect, those shaking variations related to the two horizontal velocity components, x and y, are also shown in Figure 5.

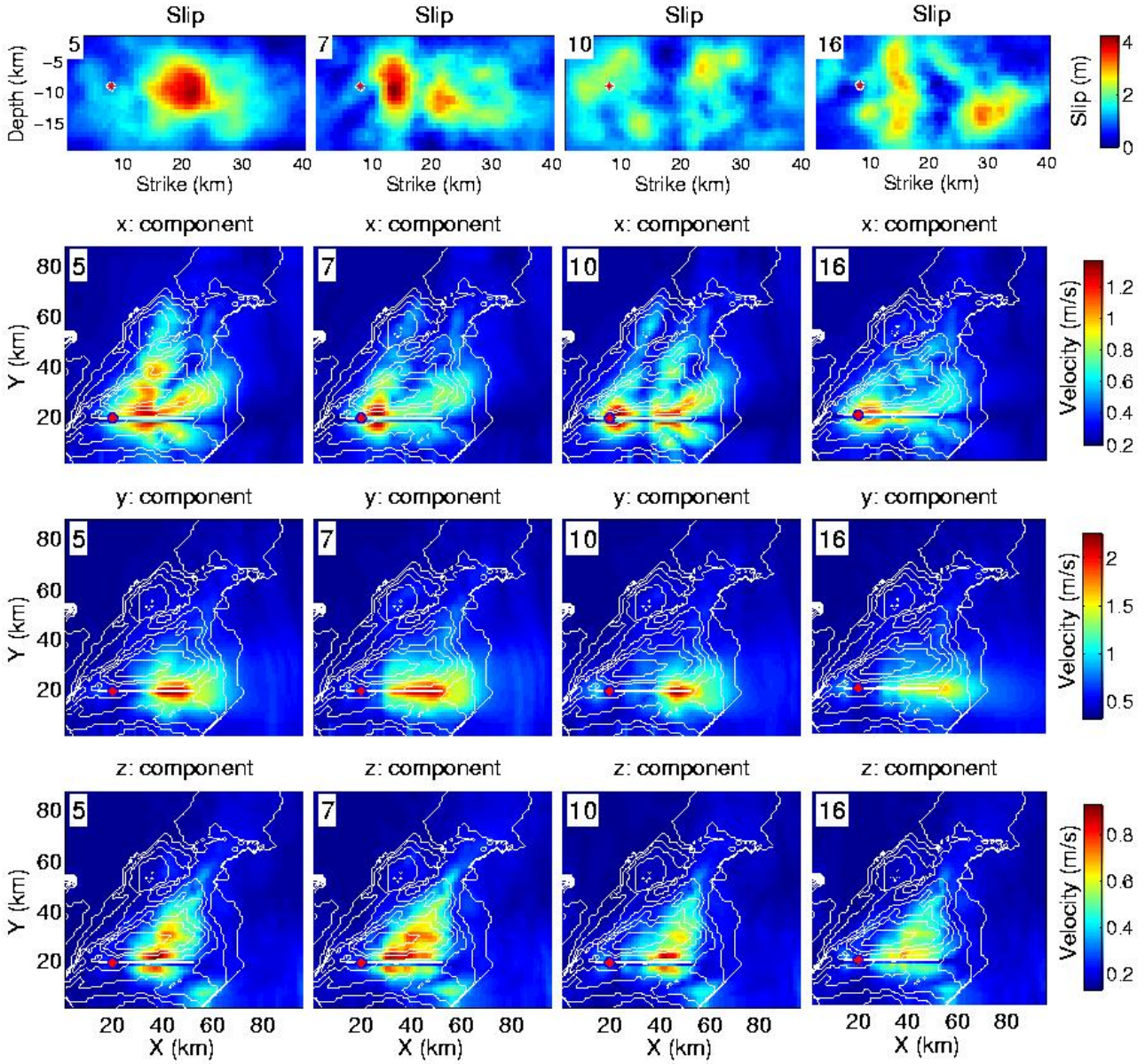

Figure 4: Peak ground velocity distributions for slip 5, 7, 10 and 16 for all three components. The corresponding slip distributions are shown at the top.

The largest PGV standard deviation of the x-component (Figure 5, bottom left, 0.25 m/s), is observed in the area near the epicenter. A directivity effect is not visible even in the far end area of the fault. The basin structure and the slip histories seem to control the seismic motion generation. Basin-structure dependent amplification can also be seen from both the mean value and standard value of the x-component PGV distributions (Figure 5, left). This further demonstrates that directivity does have different effects on the three seismic motion components.

The maximum PGV distribution of the modulus component, i.e. the length of the velocity vector, (Figure 5, top right) looks similar to the one for the fault perpendicular component (Figure 5, top middle) both in terms of absolute maximum value and spatial pattern. We conclude that the maximum seismic motion variation on the surface is dominated by directivity. The source related variations, however, are different for the fault parallel component (Figure 5, top left) and the fault perpendicular component (Figure 5, top middle).

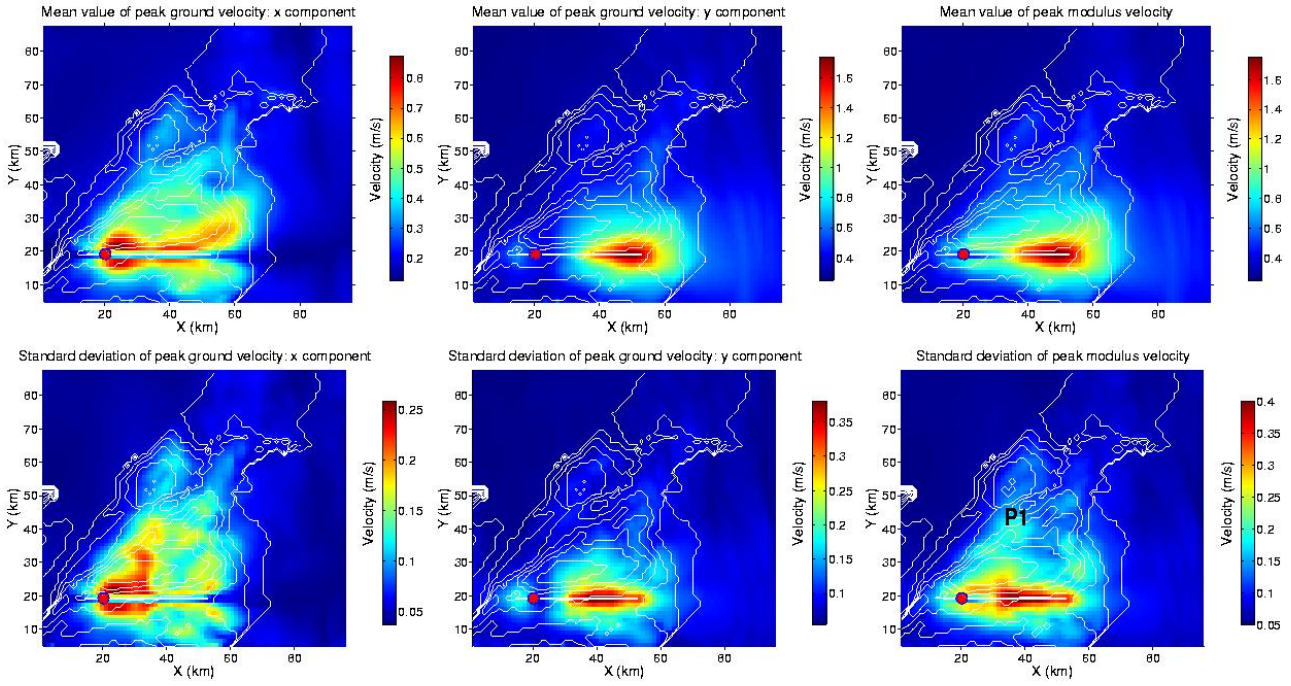

Figure 5: PGV variation, maximum and standard deviation for two horizontal and modulus component. P1 is the station with the highest ratio between the standard deviation and the mean value of PGV.

The maximum ratio between the standard deviation and the mean value for the whole area is 40%, at point P1 (Figure 5, bottom right). This value expresses in a quantitative way (limited by the number of scenarios) the source dependent PGV variations for a given M7 earthquake with the same hypocenter but varying slip histories (i.e., stress distributions prior to the event).

5. Discussions and conclusions

In this study we investigated the source dependent contribution to the strong ground motion in 3-D media with specific application to a characteristic M7.0 earthquake on the NI fault in the Los Angeles basin. The fault perpendicular motion component (y) generates at least two times larger peak velocity amplitudes than the fault parallel components (x, z) in the area around the right part of the fault, that is, in the direction towards which the rupture is propagating. This phenomenon is also observed in the strong ground motion measurement and is a crucial aspect in earthquake hazard and risk analysis.

Seismic shaking variations due to various rupture processes are also investigated in this study. The static slip (input parameter for finite source simulations) is important when calculating seismic motions because the area with large static slip (asperity area) will introduce elevated seismic motions. In combination with directivity, it can increase the complexity of surface seismic shaking.

Comparing the modulus component of PGV with those of the two horizontal components for a M7 strike-slip earthquake, we conclude that the modulus component is dominated by the fault perpendicular component.

Wang *et al*. (2006) investigated the hypocenter location effect on the seismic shaking for a constant slip distribution. The ratio between standard deviation and the mean value

of PGV (modulus component) was found to be large at the basin edge and at the two tips of fault (where directivity effect is largest) with values around 53% which is a little larger than the one (slip history effect) found in this study (40%). The different effect due to directivity and slip history, respectively, should be considered when doing ground motion prediction, at least in our specific case, that is, NI fault and LA basin.

The results shown here indicate that to reliably estimate shaking hazard for specific earthquake scenarios, the source dependent effects should be taken into account. This necessitates calculation of many different slip histories to fully account for the associated uncertainties. In the (long-) period range considered in this paper there is a marked difference between the finite-source effects on the various motion components, mixed with effects of the 3-D structure. More simulations will be necessary in the future to quantitatively estimate the contributions of small scale structures and source effects at higher frequencies.

6. Acknowledgements

We acknowledge funding from the International Quality Network - Georisk (German Academic Exchange Service), and the Elite Graduate College THESIS (Bavarian Government). We also acknowledge support from the European Human Resources Mobility Program (Research Training Network SPICE) and the provision of computational resources through the Leibniz Computing Centre Munich. ME was funded by the KONWIHR project and a stipend of the MunichRe.

7. References

Aki, K. (1967). Scaling law of seismic spectrum. *J. Geophys. Res. 72*, 1217-1231.

Aki, K., and P. G. Richards, *Quantitative seismology*, 2nd Edition, University Science Books, (2002).

Anderson, J. G., International Handbook of Earthquake and Engineering Seismology, Volume 81B, Chapter 57, ISBN: 0-12-440658-0, ACADEMIC PRESS, (2003).

Anderson, J. G. and J. E. Luco (1983a). Parametric study of near-field ground motion for a strike slip dislocation model. *Bull. Seism. Soc. Am. 73*, 23-43.

Anderson, J. G., and J. E. Luco (1983b). Parametric study of near field ground motions for oblique-slip and dip-slip dislocation models. *Bull. Seism. Soc. Am. 73*, 45-57.

Archuleta, R. J. (1984). A faulting model for the 1979 Imperial Valley earthquake, *J. Geophys. Res.*, *89*, 4559 - 4585.

Archuleta, R. J. and S. H. Hartzell (1981). Effects on fault finiteness on near-source ground motion. *Bull. Seism. Soc. Am. 71*, 939-957.

Bennett, R. A., R. E. Reilinger, W. L. Rodi, Y. Li, M. N. Toksoz, and K. W. Hudnut (1995). Coseismic fault slip associated with the 1992 Mw = 6.1 Joshua Tree, California, earthquake: Implications for the Joshua Tree - Landers earthquake sequence, *J. Geophys. Res., 100,* 6443 - 6461.

Beroza, G. C., and P. Spudich (1988). Linearized inversion for fault rupture behavior: Application to the 1984 Morgan Hill, California, earthquake, *J. Geophys. Res., 93*, 6275 - 6296.

Bouchon, M., M. N. Toksoz, H. Karabulut, M. P. Bouin, M. Dietrich, M. Aktar, et M. Edie (2000). Seismic imaging of the 1999 Izmit (Turkey) rupture inferred from near-fault recordings, *Geophys. Res. Lett., 27,* 3013 - 3016.

Bour, M. and M. Cara (1997), Test of simple empirical green's functions method on moderate-sized earthquakes, *Bull. Seism. Soc. Am., 87*, 668-683.

Collino F. and C. Tsogka (2001), Application of the PML absorbing layer model to the linear elastodynamic problem in anisotropic heterogeneous media, *Geophysics, 66,* 294-307.

Ewald, M., Igel, H., Hinzen, KG, and F. Scherbaum (2006). Basin-related effects on ground motion for earthquake scenarios in the Lower Rhine Embayment, *Geophys. J. Int.*, in print.

Grant, L. B., and P. M. Shearer (2004), Activity of the offshore Newport - Inglewood Rose Canyon fault zone, coastal Southern California, from relocated microseismicity, *Bull. Seism. Soc. Am., 94,* 747-752.

Gottschämmer, E. and K. B. Olsen (2001), Accuracy of explicit planar free-surface boundary condition implemented in a fourth-order staggered-grid velocity-stress finite-difference scheme, *Bull. Seism. Soc. Am., 91*, 617-623.

Guatteri, M., P. M. Mai, and G. C. Beroza (2005), A pseudo-dynamic approximation to dynamic rupture models for strong ground motion prediction, *Bull. Seism. Soc. Am., 94,* 2051-2063.

Haskell, N. A. (1969). Elastic displacements in the near-field of a propagating fault. *Bull. Seism. Soc. Am. 59*, 865-908.

Hauksson. E., and S. Gross (1991), Source parameters of the 1933 Long Beach earthquake, *Bull. Seism. Soc. Am., 81*, 81-98.

Herrero, A., and P. Bernard (1994). A kinematic self-similar rupture process for earthquakes, *Bull. Seism. Soc. Am., 84,* 1216 - 1228.

Hutchings, L., and F. Wu (1990), Empirical Green's functions from small earthquakes ― a waveform study of locally recorded aftershocks of the San Fernando earthquake, *J. Geophys. Res., 95*, 1187-1214.

Igel, H., P. Mora, B. Riollet (1995), Anisotropic wave propagation through finite-difference grids, *Geophysics, 60,* 1203-1216.

Joyner, W. B. and D. M. Boore (1986), On simulating large earthquakes by Green's-function addition of smaller earthquakes. *Earthquake Source Mechanics, Geophysical Monograph No. 37 (Maurice Ewing, ed.), 8,* 269 - 274.

Kanamori, H. (1977), The energy release in great earthquakes, *J. Geophys. Res., 82*, 2981 - 2987, 1977.

Kohler, M., H. Magistrale, and R. Clayton (2003), Mantle heterogeneities and the SCEC three-dimensional seismic velocity model version 3, *Bull. Seism. Soc. Am., 93*, 757-774.

Kohrs-Sansorny, C., F. Courboulex, M. Bour and A. Deschamps (2005). A Two-stage method for ground-motion simulation using stochastic summation of small earthquakes, *Bull. Seism. Soc. Am., 95*, 1387-1400.

Larsen, S., R. Reilinger, H. Neugebauer, and W. Strange (1992). Global Positioning System measurements of deformations associated with the 1987 Superstition Hills earthquake: Evidence for conjugate faulting, *Geophys. Res.*, 97, 4885 - 4902.

Marcinkovich, C., and K. B. Olsen (2003), On the implementation of Perfectly Matched Layers in a 3D fourth-order velocity-stress finite-difference scheme, *J. Geophys. Res., 108*, 2276-2293.

Olsen, K. B. (2000), Site amplification in the Los Angeles basin from 3D modelling of ground motion, *Bull. Seism. Soc. Am. 90*, S77-S94.

Olsen, K. B. and R. J. Archuleta (1996). 3D-simulation of earthquakes in the Los Angeles fault system, *Bull. Seism. Soc. Am. 86*, 575-596.

Somerville, P. G., N. F. Smith, R. W. Graves, and N. A. (1997). Modification of empirical strong ground motion attenuation relations to include the amplitude and duration effects of rupture directivity. *Seism. Res. Lett. 68*, 199-222.

Wang, H.J., H. Igel, A. Cochard and M. Ewald (2006), Numerical Green's Functions for Sub-Faults in 3-D: Application to the Newport-Inglewood Fault, Los Angeles Basin, submitted to Bull. Seis. Soc. Amer.

Wells, D. L., and J. K. Coppersmith (1994), New empirical relationships among magnitude, rupture length, rupture width, rupture area, and surface displacement, *Bull. Seism. Soc. Am. 84*, 974-1002.